THE JOURNAL OF PHYSICAL CHEMISTRY B

Article

pubs.acs.org/JPCB

Analysis of Confined Random Walkers with Applications to Processes Occurring in Molecular Aggregates and Immunological Systems

Matthew Chase,*,† Kathrin Spendier,*,‡ and V. M. Kenkre*,†

†Consortium of the Americas for Interdisciplinary Science and the Department of Physics and Astronomy, University of New Mexico, Albuquerque, New Mexico 87131, United States

‡BioFrontiers Center and Department of Physics and Energy Science, University of Colorado at Colorado Springs, Colorado Springs, Colorado 80918, United States

Text

ABSTRACT: Explicit solutions are presented in the Laplace and time domains for a one-variable Fokker–Planck equation governing the probability density of a random walker moving in a confining potential. Illustrative applications are discussed in two unrelated physical contexts: quantum yields in a doped molecular crystal or photosynthetic system, and the motion of signal receptor clusters on the surface of a cell encountered in a problem in immunology. An interesting counterintuitive effect concerning the consequences of confinement is found in the former, and some insights into the driving force for microcluster centralization are gathered in the latter application.

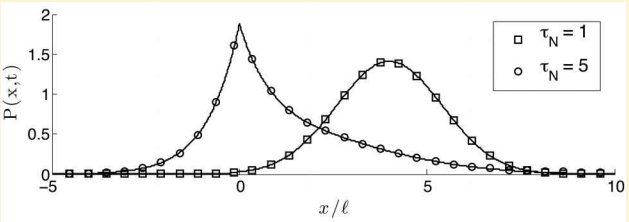

1. INTRODUCTION AND THE STARTING EQUATION

Random walks of moving particles or excitations are ubiquitous in nature. In some of the cases, the walkers are subjected to forces that confine them to a given region in space. Examples of the latter situation are found in a variety of microscopic and macroscopic systems and phenomena including artificial photosynthetic machines, enzyme ligand binding, home range formation in animal behavior, and flocking.[1−5] Their theoretical study has often employed a Fokker–Planck equation in the Smoluchowski form which, in a simple 1-dimensional context, is

$$\frac{\partial P(x,t)}{\partial t} = \frac{\partial}{\partial x}\left(\frac{dU(x)}{dx}P(x,t)\right) + D\frac{\partial^2 P(x,t)}{\partial x^2} \tag{1}$$

The equation governs the time evolution of the probability density $P(x,t)$ that a 1-dimensional random walker is at position x at time t, with D being the diffusion constant and $U(x)$ the confining potential. It is obtained in the usual manner[6,7] as a consequence of an appropriate Langevin equation for the random walker in a highly damped environment with white noise. The term "Smoluchowski equation" is used particularly when $U(x)$ is taken to be quadratic in x. The quadratic nature of the assumed potential arises from the standard usage of harmonic oscillators in science and from familiarity with its consequences.

Our interest in this article is in investigating random walks in potentials that confine but are *not quadratic* in the distance from the attractive center. Whereas higher powers in x present situations that are not analytically tractable, the case of a potential linear in x can be solved explicitly as we show below. The solutions are simple but not trivial. They possess features, some of which are, perhaps surprisingly, richer in content than those for quadratic potentials. One such (striking) feature is that, starting from a localized (δ-function) initial distribution, the probability density *changes its shape* as it proceeds toward its final steady state form around the attractive center. By contrast, the normally used quadratic potential forces a single (Gaussian) shape on the probability density for all time. The shape changes only its width as it proceeds to the steady state form. The difference has discernible consequences on the time evolution of derived quantities such as the average position and velocity of the walker. Our interest is in piecewise linear potentials $U(x)$. Fully analytic solutions are possible for a pair of symmetrical linear pieces while seminumerical work becomes necessary for multiple pieces.

The potential we study analytically is proportional to $|x|$, i.e., consists of two linear pieces of equal and opposite slopes on the two sides of an attractive center (taken to lie at $x = 0$). Consequently, the equation that is our starting point is

$$\frac{\partial P(x,t)}{\partial t} = \Gamma\frac{\partial}{\partial x}\left(\frac{|x|}{x}P(x,t)\right) + D\frac{\partial^2 P(x,t)}{\partial x^2} \tag{2}$$

where Γ is the strength of the potential with units of velocity.

Discussion of features of the solutions of eq 2 and presentation of two applications, one to the problem of calculating quantum yield in a doped molecular crystal, and the other a study in immunology, specifically regarding the motion of signal receptor clusters on the surface of a cell, are the reason for this report. We have learned after we completed our work that the dynamics of a particle in a subquadratic potential have been known in part earlier, with a partial solution to (eq 2) having been given by Smoluchowski[8] for the case of a reflecting

Received: December 22, 2015
Revised: February 15, 2016

   DOI: 10.1021/acs.jpcb.5b12548

boundary at $x = 0$ and extended by Lamm and Schulten[9−11] to absorbing boundary conditions. However, our solution that we present here covers the entire real line and is for *arbitrary* initial conditions. Furthermore, we give the propagator in both time- and Laplace-spaces, with the latter being directly useful for reaction-diffusion problems. These features and the illustrative applications we have provided are the reasons behind reporting this study. The application envisaged to quantum yield calculations in a doped molecular crystal[12−14] is to an experiment that can be performed in principle. The application to the immunological problem is to experiments already performed but is illustrative in the sense that we do not present quantitative fits to observations but rather provide a qualitative analysis from our solutions.

2. SOLUTIONS AND THEIR BEHAVIOR

We first notice that the steady state distribution of eq 2, $P_{SS}(x)$, may be obtained by putting its left-hand side equal to zero:

$$P_{SS}(x) = \lim_{t\to\infty} P(x, t) = \frac{1}{2l} e^{-|x|/l} \tag{3}$$

Here $l = D/\Gamma$ is the characteristic width of the distribution.

Our interest is in the full time dependence of the solutions of eq 2, consequently in an explicit expression for the propagator $\Pi(x, x_0, t)$, i.e., the solution for the probability density at x at a time t later given that the initial density is localized at x_0. For this purpose we use Laplace transforms. When applied to eq 2 with the localized initial condition $P_0(x) = \delta(x - x_0)$, they yield

$$\epsilon\tilde{P}(x, \epsilon) - \delta(x - x_0) = \Gamma\frac{d}{dx}\left(\frac{|x|}{x}\tilde{P}(x, \epsilon)\right) + D\frac{d^2\tilde{P}(x, \epsilon)}{dx^2} \tag{4}$$

where ϵ is the Laplace variable and tildes denote transforms. We consider $x_0 > 0$, with the case of $x_0 < 0$ being solved by symmetry and consequently by a simple $x \to -x$ transformation. We note that the domain of x naturally breaks up into three different regions separated by two points of discontinuity, the first at $x = 0$ due to the potential, the second at x_0 due to the initial condition. Within each of these regions, the equation becomes a second order ODE with constant coefficients suggesting an ansatz of the form $\tilde{P}(x, \epsilon) \sim e^{\lambda x}$. This leads to an expression of the form

$$\tilde{P}(x, x_0, \epsilon) = \mathcal{A}e^{\left(\pm 1+\sqrt{1+\frac{4l\epsilon}{\Gamma}}\right)(x/2l)} + \mathcal{A}'e^{\left(\pm 1-\sqrt{1+\frac{4l\epsilon}{\Gamma}}\right)(x/2l)}$$

Here + (−) corresponds to $x < 0$ ($x > 0$) and $\mathcal{A}$ and $\mathcal{A}'$, constants determined by matching at the boundary conditions, incorporate the discontinuities' effects. The requirement that $\tilde{P}(x, x_0, \epsilon)$ must vanish as $x \to \pm\infty$ eliminates two of the constants. Equality of the probability density on the left and the right at each boundary and the requirement that the integral of eq 4 around each discontinuity goes to zero as the integral limits approach the discontinuity determine the four remaining constants. Application of these boundary conditions, along with removing the requirement that $x_0 > 0$, yields the propagator $\tilde{\Pi}(x, x_0, \epsilon)$ in the Laplace domain:

$$\tilde{\Pi}(x, x_0, \epsilon) = \frac{e^{-(|x|-|x_0|)/2l}}{\Gamma\sqrt{1+\frac{4l\epsilon}{\Gamma}}}\left[e^{-\sqrt{1+\frac{4l\epsilon}{\Gamma}}|x-x_0|/2l} + \frac{e^{-\sqrt{1+\frac{4l\epsilon}{\Gamma}}(|x|+|x_0|)/2l}}{\sqrt{1+\frac{4l\epsilon}{\Gamma}}-1}\right] \tag{5}$$

Inversion of the Laplace-domain propagator into an explicit time-domain propagator is possible either through explicit Bromwich contour integrations or by reference to tables.[15] The time domain propagator is a combination of error functions, exponentials, and the Gaussian diffusion propagator modified appropriately for convection:

$$\Pi(x, x_0, t) = \frac{1}{\sqrt{4\pi Dt}}e^{-((x-x_0)^2+\Gamma^2t^2)/4Dt}e^{-(|x|-|x_0|)/2l} + \frac{e^{-|x|/l}}{4l}\left(1 - \mathrm{erf}\left(\frac{|x| + |x_0| - \Gamma t}{\sqrt{4Dt}}\right)\right) \tag{6}$$

Our analytic results (eq 6) can be verified easily through a numerical solution of eq 2. The latter can be thought of as the continuum limit of

$$\frac{dP_m(t)}{dt} = F(P_{m+1} + P_{m-1} - 2P_m) + f\left(\frac{|m+1|}{m+1}P_{m+1} - \frac{|m-1|}{m-1}P_{m-1}\right) \tag{7}$$

where $P_m(t)$ is the probability of occupation of the mth site at a time t in a discrete 1-dimensional lattice, F is the nearest neighbor hopping rate, and f is the rate of motion toward the attractive center at $m = 0$. If a is the lattice spacing, the continuum limit

$$a \to 0,\ F \to \infty,\ f \to \infty,\ Fa^2 \to D,\ 2fa \to \Gamma$$
$$ma \to x,\ P_m(t)/a \to P(x, t)$$

converts eq 7 into eq 2. We use $m_0 = x_0/a$ and the above discretized forms of Γ and D to represent eq 6, the propagator derived analytically in its discrete version, as

$$\Pi_{m,m_0}(t) = \frac{1}{\sqrt{4\pi Ft}}e^{-((m-m_0)^2+4f^2t^2)/4Ft}e^{-f(|m|-|m_0|)/F} + \frac{f}{2F}e^{-2f|m|/F}\left(1 - \mathrm{erf}\left(\frac{|m| + |m_0| - 2ft}{\sqrt{4Ft}}\right)\right) \tag{8}$$

We compare our analytic solution in eq 8 (solid lines) with the numerical solution (markers) of the discretized differential equation, obtained using standard Matlab procedures such as ODE45. Displayed in Figure 1 is the spatial distribution at two widely different times. The first depicts an early situation close to the initial distribution, and the second is a late situation near the steady state. The dimensionless time τ_N is Ft in units of 4×10^6. It has the respective values 1 and 5 for the two cases shown in Figure 1. The value of f/F we have taken is 0.25×10^{-3}, and the number of lattice sites is 1200. Agreement is excellent given that we have used the size of the region to be large relative to the equilibrium width l and that the potential (which we will call V-potential in the rest of this paper) is not too steep. The transition between an initial Gaussian and the eventual cusped

DOI: 10.1021/acs.jpcb.5b12548

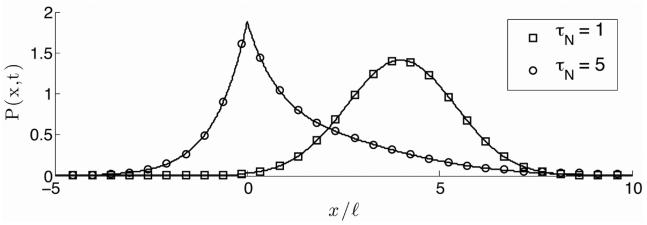

Figure 1. Comparison of our analytic solution in eq 8 (solid lines) with numerically obtained counterparts (markers) showing excellent agreement at two different dimensionless times $\tau_N = 1$ and $\tau_N = 5$. Here τ_N is Ft in units of 4×10^6; there are 1200 sites in the chain and $f/F = 0.25\times 10^{-3}$. The walker location was at a distance $x_0/l = 5$ initially. The shape-shifting of the solution is also clear from an early time Gaussian to a late time mod exponential.

steady state distribution (a decaying exponential) provides much of the interesting behavior of our solutions.

2.1. Shape-Shifting of the Solutions. Insight into the solutions of our Fokker–Planck equation, eq 2, can be gained by analyzing the two terms in eq 6. The first term, essentially a Gaussian, is characteristic of diffusion. The second term has the spatial form of an exponential decay required by the steady state distribution. The peak of the Gaussian travels ballistically after the manner of the case when the potential has a simple bias, i.e., $U(x) = \pm\Gamma x$. The bias respects the potential experienced on either side of the confining center. It causes the peak of the Gaussian term to move through the center. At long times, only the tail contributes to the probability distribution. Note that the decaying exponential determines the long time behavior of the propagator and is modified by an error function.

In order to examine more closely the passage from the initial shape through the Gaussian intermediate to the final exponential form, we display Figure 2. Initially, the probability

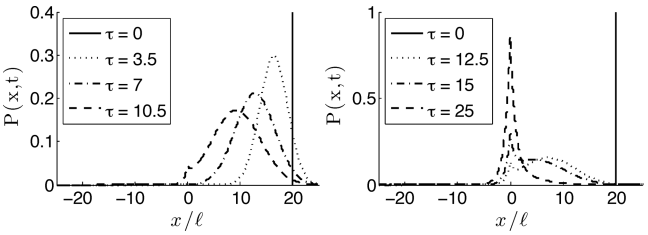

Figure 2. Time evolution of the probability density for a walker localized initially at $x_0/l = 20$. (Dimensionless) time is measured as the ratio of t to $\sqrt{2D/\Gamma^2}$, with three early values (3.5, 7, 10.5) being depicted in the left panel and three late values (12.5, 15, 25) in the right panel. The initial value is displayed in both for comparison. The left panel shows that the distribution changes from localized through Gaussians as the walker moves ballistically toward the attractive center and diffuses simultaneously. The last curve shows a little peak at the attractive center as the walker begins to settle at the attractive center. In the right panel the peak grows as the shape changes clearly into the mod exponential. Shape shifting is particularly clear in this figure.

distribution travels ballistically maintaining the shape of a Gaussian. However, when the probability of the walker being at the potential center reaches an appreciable value, the distribution begins to form a cusp, reflecting the approach toward the steady state distribution. Following the formation of the cusp, the distribution rapidly transitions into an intermediate state reflecting both the traveling Gaussian and the exponential. During this transition period there are two local maxima. Finally, the long-term steady state distribution is attained. Needless to state, the shape-shifting and the final shape follow from the fact that the random walkers relax to their equilibrium distribution appropriate to whatever potential the walkers move in. The quadratic potential provides an exceptional case wherein the shape maintains itself Gaussian at all times.

2.2. Average Position and Velocity. Additional insight into the consequences of the random walker moving in a V-potential can be obtained by exploring its average position $\langle x\rangle$ and its average velocity $\langle v\rangle \equiv \mathrm{d}\langle x\rangle/\mathrm{d}t$. With a positive value chosen for x_0, the former is obtained by simply calculating the moment of the propagator as given by our eq 6:

$$\langle x\rangle = \left(\frac{x_0 - \Gamma t}{2}\right)\left[1 + \mathrm{erf}\left(\frac{x_0 - \Gamma t}{\sqrt{4Dt}}\right)\right] + \left(\frac{x_0 + \Gamma t}{2}\right)\left[1 - \mathrm{erf}\left(\frac{x_0 + \Gamma t}{\sqrt{4Dt}}\right)\right]\mathrm{e}^{x_0/l} \tag{9}$$

The expression for the average position consists of a term showing ballistic motion to the left and a term showing ballistic motion to the right, both at speed Γ, and both modified by error function factors representative of simultaneous diffusion with diffusion constant D. At long times, the combination of the two terms results in $\langle x\rangle \to 0$. Time differentiation gives

$$\frac{\mathrm{d}\langle x\rangle}{\mathrm{d}t} = \langle v\rangle = -\frac{\Gamma}{2}\left[1 + \mathrm{erf}\left(\frac{x_0 - \Gamma t}{\sqrt{4Dt}}\right) - \left(1 - \mathrm{erf}\left(\frac{x_0 + \Gamma t}{\sqrt{4Dt}}\right)\right)\mathrm{e}^{x_0/l}\right] \tag{10}$$

Equations 9 and 10 apply for $x_0 > 0$. The average velocity obviously begins as the slope of the V-potential at the position of initial placement, i.e., has the value $-\Gamma$. If there were no diffusion, i.e., if $D = 0$, the average velocity would jump to zero when the walker reaches the attractive center as a consequence of the reverse sign of the V-potential slope on the other side of the center. Diffusion smooths the jump. The sum of the first two terms inside the square brackets in eq 10 starts at the value 2 and drops to 0 while the third term vanishes both initially and finally. The error functions ensure that there is dormant behavior at small times during which the velocity is essentially at the original constant value until diffusion kicks in and the velocity starts dropping. This can be seen in Figures 3 and 4 where we plot $\langle v\rangle/\Gamma$ against a dimensionless time.

In Figures 3 and 4, we explore the effect of varying each of the parameters, D, Γ, and x_0, on the average velocity of the confined random walker. The time scale is chosen separately in the case of each parameter, and the plots are parametrized by $\alpha \equiv x_0/l$, the ratio of the initial position to the steady state width of the distribution. The effect of changing Γ is shown on the left in Figure 3, where an increase in Γ corresponds to an increase in α. In the short term, shown in the inset, the walker travels ballistically for a longer time when the potential steepness is decreased. The long-term decay into the steady state probability distribution, indicated by $\langle v\rangle/\Gamma \to 0$, occurs more slowly for a decreased potential strength. These results match with the intuitive effect of a steeper potential in that the walker will initially travel toward the potential center at a larger velocity, experiencing the effects of confinement earlier

DOI: 10.1021/acs.jpcb.5b12548

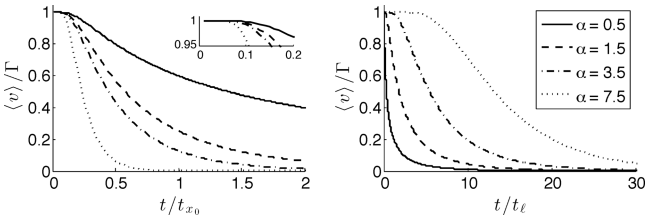

Figure 3. Dependence of the velocity of the random walker on time showing the effect of changing the potential slope Γ (left panel) and the initial location x_0 (right panel). The parameter that is varied and shown in the legend in the right panel, $\alpha \equiv x_0/l$, applies to given line styles in both panels. The dimensionless time used is t/t_{x_0} in the left panel and t/t_l in the right. Here $t_{x_0} = {x_0}^2/2D$ and $t_l = l^2/2D$ are times taken by a pure diffusive walker to cover distances x_0 and l, respectively. The left panel includes an inset showing the short-term ballistic behavior where a dormant stage is followed by a velocity decrease.

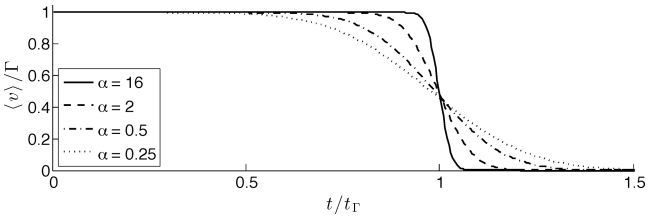

Figure 4. Effect of the diffusion constant D, in the form of the dimensionless parameter $\alpha \equiv x_0/l = x_0\Gamma/D$, on the time evolution of the velocity of the random walker. The dimensionless time used here is t/t_Γ where $t_\Gamma \equiv x_0/\Gamma$ is the time it takes a purely ballistic walker with velocity Γ to travel a distance x_0. Note that all curves intersect at the same point when t equals t_Γ.

allowing it to more quickly settle into the steady state distribution. Overall, increasing the potential strength will decrease the transition time from initial ballistic motion to the final steady state distribution.

The effect of changing the initial position of the particle, x_0, is shown in the right panel of Figure 3. While the behavior appears similar to that shown in the left panel, it is to be noted that the time spent in the initial ballistic motion increases as the random walker is initially placed further from the potential center. The walker approaches its steady state distribution more slowly when initialized further away. The α values displayed in the right panel apply to both panels with their associated line types, so we see that that an increase in α moves one in opposite order among the curves in the two panels. The effect of changing the diffusion constant, where an increase in D corresponds to a decrease in α, is displayed in Figure 4. A larger diffusion constant allows the walker to sense the confinement earlier but makes it spend less time relatively moving ballistically. This combination has the consequence that the decay into the steady state is slower. In effect, a large diffusion constant extends the time under which the walker transitions from the initial ballistic motion into the steady state. Note that all the curves in Figure 4 intersect in a single point at $t = t_\Gamma$.

We also show the relation between $\langle x\rangle$ and $\langle v\rangle$ in part because observations have been reported in that manner in the study of immunological synapse formation, a subject we passingly address in section 5. Although we have not obtained such a relation by analytic means, eliminating the time dependence is possible numerically. The results for changing Γ are depicted in Figure 5 (effect of changing x_0 is identical). Increasing α, corresponding to an increase in either Γ or in x_0, leads to the walker traveling ballistically for a longer distance before slowing down into the steady state. As α is decreased, this plunge has qualitatively different shapes, with curve convexity increasing, and indicates a sharper initial slowdown followed by a more leisurely approach to the steady state.

The effect of changing D is depicted in Figure 5, where an increase in D corresponds to a decrease in α. Decreasing the diffusion constant makes the walker travel a larger distance ballistically before reaching the $\langle x\rangle = 0$ region. The plunge occurring closer to the confining center for larger D suggests that diffusion acts as a sensing mechanism for the walker, allowing it to interact with the potential discontinuity while further away.

3. COMPARISON WITH THE QUADRATIC POTENTIAL

What are the essential differences between confined random walkers obeying eq 2 that we have been analyzing in this paper, i.e., obeying the general eq 1 with the V-potential as $U(x)$ on one hand, and those obeying eq 1 with the commonly used (see, e.g., ref 16) quadratic $U(x)$ given by $(1/2)\gamma x^2$ on the other? This is the question we examine more closely in this section. For this purpose we compare the propagator we have derived for the case of the V-potential, eq 6, with the well-known quadratic Smoluchowski propagator[6,7,16]

$$\Pi(x, x_0, t) = \frac{e^{-(x-x_0e^{-\gamma t})^2/4D\mathcal{T}(t)}}{\sqrt{4\pi D\mathcal{T}(t)}}, \qquad \mathcal{T}(t) = \frac{1 - e^{-2\gamma t}}{2\gamma} \tag{11}$$

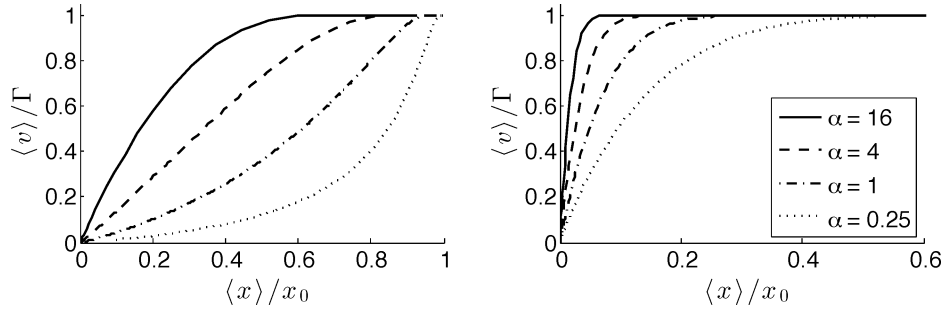

Figure 5. Relation between the velocity (time derivative of average displacement) and the displacement of the random walker. Plotted is $\langle v\rangle/\Gamma$ versus $\langle x\rangle/x_0$ when Γ (left) and D (right) is varied, both in the form of the dimensionless parameter $\alpha \equiv x_0/l = x_0\Gamma/D$. Note the change in the convexity of the curves in the left panel.

DOI: 10.1021/acs.jpcb.5b12548

The spatial dependence of the propagator is always Gaussian in the quadratic case. Consequently, the shape-shifting phenomenon we have witnessed for the V-potential case does not arise in the quadratic case. Additionally, the average displacement and velocity, $\langle x\rangle$ and $\langle v\rangle$, have forms for the quadratic case that are considerably simpler than for the V-potential. In the quadratic case they are easily calculated to be exponential in time, $\langle x\rangle = x_0 e^{-\gamma t}$, $\langle v\rangle \equiv d\langle x\rangle/dt = -x_0\gamma e^{-\gamma t}$, and thus to be related linearly to each other: $\langle v\rangle = -\gamma\langle x\rangle$. The time dependence of $\langle x\rangle$ and $\langle v\rangle$ is, on the other hand, more complex for the V-potential, see eqs 9 and 10. Unlike in the quadratic case, it is not straightforward at all to eliminate t from those equations to obtain a v−x relation. We found it necessary to use a numerical procedure to extract that relation. Unlike in the quadratic case, there is an unavoidable dependence of the V-potential relation on the diffusion constant D and the initial location x_0.

The difference in the initial slopes of the velocity versus time plots in the quadratic versus the V-potential (eq 10) case deserves particular mention. Being $-x_0\gamma$ in the quadratic case, the slope is dependent on the potential strength, and is different for different initial locations. Neither the initial location nor any potential parameter decides the initial slope in the V-potential case, with the $v(t)$ curve being initially *totally* flat in the V-potential case. Not only the first t-derivative but *all* order derivatives of the velocity vanish initially. This is confirmed explicitly by differentiating eq 10

$$\frac{d\langle v\rangle}{dt} = \frac{x_0\Gamma}{\sqrt{4\pi D t^3}} e^{-(x_0-\Gamma t)^2/4Dt}$$

and noticing that, at $t = 0$, the Gaussian term vanishes faster than any purely polynomial term can grow. As repeated differentiations only result in polynomials of larger (finite) order, all derivatives of $\langle v\rangle$ vanish at $t = 0$, which provides the totally flat nature of the velocity curve initially. This dormant behavior comes from the presence of an isolated essential singularity and is similar to what happens in the context of Arrhenius (activated) dependence of chemical rates or the Einstein specific heat if the temperature T is the abscissa rather than the time t as here.

By multiplying eq 1, integrating over all x, and invoking standard boundary conditions on $P(x)$ and its spatial derivatives, one can write, for any potential $U(x)$

$$\frac{d\langle x\rangle}{dt} = \langle v\rangle = \left\langle -\frac{dU(x)}{dx}\right\rangle \tag{12}$$

In the quadratic case, the force or velocity $dU(x)/dx$ is linear in x, but in the V-potential case, it is highly nonlinear, being proportional to $|x|/x$. The linearity in the former case ensures that a closed differential equation for $\langle x\rangle$ exists. In the latter case it does not exist and so D has an effect on the average velocity. It is the fact that the relation $\langle f(x)\rangle = f(\langle x\rangle)$ is *by no means valid* for such nonlinear functions $f(x)$ that is responsible for the richer consequences of the V-potential. In the quadratic case, the linearity of the force validates the relation accidentally and thereby imposes a simple relation between $\langle v\rangle$ and $\langle x\rangle$ without any influence of the diffusion constant.

4. APPLICATION TO QUANTUM YIELD CALCULATIONS IN DOPED MOLECULAR CRYSTALS

As one of the two illustrative applications of our calculations based on the V-potential we have studied, we describe in this section quantum yield calculations in doped molecular crystals[12−14] and photosynthetic systems.[18] In order to study the magnitude and nature of exciton motion in organic crystals such as anthracene, guest molecules such as those of tetracene are introduced in small concentrations in the host crystal. Light is made to shine and produce Frenkel excitations that travel within the host and are captured by the guest molecules (also called traps). The situation is similar in photosynthetic systems where the traps are the reaction centers where the excitation is caught and used for the process of making sugar.[18]

Electronic excitations have a finite lifetime (different for the host and the guest) as they decay giving rise to radiation, at different frequencies for the host and the guest so that one can keep track of how many of the excitations placed originally into the host by illumination have been caught by, and emerged from, the guest. The ratio of the number eventually emerging from the host to the number originally placed in the host is known as the (host) yield and often denoted by ϕ. If there are no nonradiative processes the guest yield is $1 - \phi$ and the (dimensionless) energy transfer rate is often said to be $(1 - \phi)/\phi$. We calculate these quantities in the presence of our V-potential in a representative 1-dimensional molecular crystal. The starting equation is given by eq 2 with additional decay and capture terms

$$\frac{\partial P(x,t)}{\partial t} + \frac{P(x,t)}{\tau} = \Gamma\frac{\partial}{\partial x}\left(\frac{|x|}{x}P(x,t)\right) + D\frac{\partial^2 P(x,t)}{\partial x^2} - C\delta(x - x_r)P(x,t) \tag{13}$$

where τ is the lifetime, C is the capture parameter, x_r is the trap site, and

$$\phi = 1 - \frac{e^{-(|x_r|-|x_0|)/2l}\left[\left(\sqrt{1+\frac{4l}{\Gamma\tau}}-1\right)e^{-\sqrt{1+\frac{4l}{\Gamma\tau}}|x_r-x_0|/2l} + e^{-\sqrt{1+\frac{4l}{\Gamma\tau}}(|x_r|+|x_0|)/2l}\right]}{\frac{\Gamma\sqrt{1+\frac{4l}{\Gamma\tau}}\left(\sqrt{1+\frac{4l}{\Gamma\tau}}-1\right)}{C} + \sqrt{1+\frac{4l}{\Gamma\tau}} - 2e^{-\sqrt{1+\frac{4l}{\Gamma\tau}}|x_r|/2l}\sinh\sqrt{1+\frac{4l}{\Gamma\tau}}\frac{|x_r|}{2l}} \tag{14}$$

We assume that the trap site is at $x_r = L/2$ and calculate the yield for the illustrative localized initial condition that the excitation is (initially) at $x_0 = -L/2$. For such symmetrical positioning around the origin, the yield becomes

$$\phi = 1 - \frac{\sqrt{1+\frac{4l}{\Gamma\tau}}e^{-\sqrt{1+\frac{4l}{\Gamma\tau}}L/2l}}{\frac{\Gamma\sqrt{1+\frac{4l}{\Gamma\tau}}\left(\sqrt{1+\frac{4l}{\Gamma\tau}}-1\right)}{C} + \sqrt{1+\frac{4l}{\Gamma\tau}} - 2e^{-\sqrt{1+\frac{4l}{\Gamma\tau}}L/4l}\sinh\sqrt{1+\frac{4l}{\Gamma\tau}}\frac{L}{4l}} \tag{15}$$

Let us focus our attention on the effect on the observable ϕ of the degree of confinement imposed on the excitation motion by the V-potential. The dependence of the quantum yield on Γ is depicted in Figures 6 and 7. Figure 6, where eq 15 is plotted for four values of the lifetime τ (in units of $L^2/2D$), over a range of the potential strength Γ (in units of $2D/L$), clearly shows nonmonotonic behavior: there is a minimum in the quantum yield (in Figure 6 it happens to appear between the values 1 and 2 of the abscissa). Since the curves rise on both sides of this value, we see that the quantum yield is nonmonotonic in the confinement strength. This remarkable nonmonotonicity effect has been recently reported for quadratic confinement potentials

DOI: 10.1021/acs.jpcb.5b12548

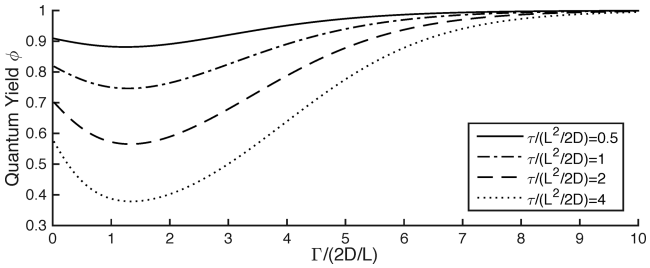

Figure 6. Nonmonotonic dependence of the quantum yield, eq 15, on the potential strength Γ (in units of $2D/L$) for four different values of the lifetime τ (in units of $L^2/2D$). Location of the trap, x_r, and the initial location of the Frenkel excitation, x_0, are separated by a distance L symmetrically around the origin. The capture parameter, C, is set to 4 (in units of $2D/L$). Nonmonotonic effects (see text) are clear from the minimum in the quantum yield located at $\Gamma \approx 2D/L$.

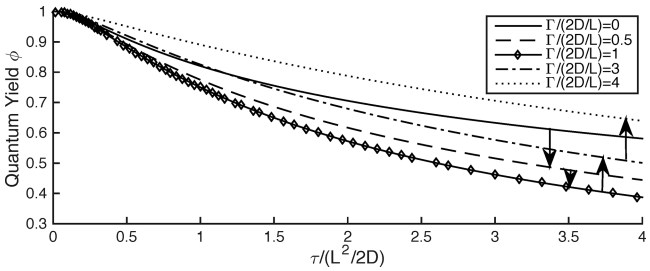

Figure 7. Nonmonotonic dependence of the quantum yield, eq 15, for five values [0.25, 0.5, 1, 2, 4] of the potential strength Γ (in units of $2D/L$) for a range of the lifetime τ (in units of $L^2/2D$). Location of the trap, x_r, and the initial localization of the Frenkel excitation, x_0, are separated by a distance L symmetrically around the origin. The capture parameter, C, is set to 4 (in units of $2D/L$). Nonmonotonicity is seen through the increase, and subsequent decrease in the normalized yield for all values of τ as Γ is increased, with the maximum occurring at $\Gamma \approx 2D/L$.

in the trapping of Smoluchowski random walkers[16] and in the transmission of infections in epidemics.[17]

The nonmonotonicity effect can also be seen directly in the time-domain.[16,17] In our present context, this behavior can be noticed in the variation of the quantum yield on the lifetime of the excitation. This is clear in Figure 7, where the dependence of ϕ on τ is shown for five values of the confinement strength Γ. The lifetime, scaled to the time the excitation would take to traverse as a random walker the distance between the initial condition and the trap site, is plotted on the x-axis. The nonmonotonic dependence of the quantum yield on the potential strength is confirmed in the figure. The black arrows, whose direction corresponds to successively higher values of Γ, point out this nonmonotonicity as Γ is increased: initially the yield decreases, it reaches a minimum, and then it increases. Intuitively this results because, for small values of Γ, confinement helps trapping by limiting the probability of the excitation diffusing to $\pm\infty$ and hurts trapping at large values of Γ by strongly concentrating the probability that the excitation is very close to the origin.

5. POSSIBLE APPLICATION TO IMMUNOLOGICAL SYNAPSE FORMATION

A second illustrative application of our calculations based on the V-potential lies in the area of T cell-antigen recognition, specifically in the immunological synapse formation that has received much attention in the past decade. We point out our findings below; our intention is to present only qualitative arguments, not quantitative predictions or explanations.

5.1. System and Biological Questions. Many important biological processes begin when a target molecule binds to a cell surface receptor protein. This event leads to a series of biochemical reactions involving receptor and signaling molecules, and ultimately a cellular response. An important feature of such biological systems is that cell surface receptors are mobile, and their mobility is influenced by their interaction with intracellular proteins including the actin cytoskeleton. For example, the recognition of antigenic peptide by T cells in contact with antigen presenting cells (APC) entails coordinated movement of T cell receptors (TCRs) and other molecules toward the center of the T cell/APC contact region. The spatially organized configurations that result are collectively referred to as the immunological synapse[19,20] and are believed to be important for T cell proliferation, differentiation, and function.[21] However, the underlying mechanism of TCR microcluster translocation is still controversial. The biological entity that seems to provide the major driving force causing centripetal TCR microcluster motion is the retrograde flow of actin.[22−24] The actin cytoskeleton is a filamentous network known to provide mechanical forces to control different cell function including the transport of TCRs. How TCRs are connected to actin is still unclear, but it might be by a frictional coupling mechanism.[25,26] Literature suggests that two major forces can cause actin flow. It could come from actin polymerization pushing against the cell membrane.[27] It could also arise from the pulling of myosin II against the branched F-actin network.[28] Myosin II contraction[28] represents a distance-dependent force due to elevated myosin II concentration at the cell periphery compared to the cell center.[23] Although we are in no position to make definitive contributions to answering these questions, it appears that some partial headway into the problem of distinguishing between the two causes could be made with the help of our calculations.

5.2. Experimental Results and V-Potential Predictions. We focus on observations reported concerning the time and distance dependence of velocities of TCR microclusters on the surface of the cell during immunological synapse formation. Approximating the motion of the TCR microclusters as being radial allows us to use directly the 1-dimensional theoretical results obtained in our calculations. After an initial period of global cellular dynamics, the time dependence of the average velocity is observed to decay toward a zero average value.[24] This is qualitatively similar to the behavior depicted in Figures 3 and 4. However, experiment also provides the *position*-dependence of the velocity of the TCR microclusters. Using the results found in ref 30 we have reconstructed their data, see left panel in Figure 8. Two distinct regions are apparent: a central region within 4 μm of the center, and a peripheral region, outside the 8 μm diameter region. The dynamics in each region are different. In the central region, the microclusters travel slowly, approximately at 4 nm/s, with no discernible distance dependence. They travel faster in the peripheral region, at ≈20−100 nm/s, with a strong dependence on distance. This motivated us to extend our calculations by considering a piecewise linear potential which is a composite of a flat portion near the center and V-potential pieces toward the periphery. As we see below, this helps produce a velocity−distance relation that is more like the observation.

5.3. Extension of V-Potential to the Bucket Potential. The lack of distance dependence on the average velocity of the

DOI: 10.1021/acs.jpcb.5b12548

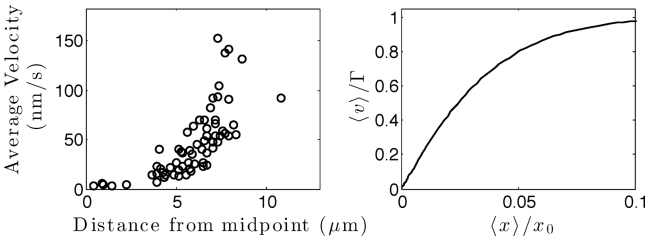

Figure 8. Qualitative comparison of experimental results (left panel) on the relation between $\langle x\rangle$ and $\langle v\rangle$ of TCR microclusters reconstructed from ref 30 with our theoretical predictions (right panel) for a V-potential. The right panel shows an increase as does the left panel, but the flat portion in the (near-origin) central region, quite obvious in the experiment, is absent in the right panel.

TCR microclusters depicted in Figure 8 suggests including a central region of constant potential (no force), i.e., where the walker dynamics are solely diffusive. As the methods used to solve eq 2 can be generalized to any linear piecewise function, we chose a potential in which we bracket the central region of no force by linear potentials with equal and opposite potential strengths:

$$U(x) = \begin{cases} \Gamma(x - L) & x > L \\ 0 & L < x < -L \\ -\Gamma(x + L) & x < -L \end{cases} \tag{16}$$

Here Γ remains the potential strength, and L is half the width of the central region of constant potential. With insertion of this "bucket" potential expression into eq 1, it is possible to proceed as in the earlier analysis and obtain the propagator.

For the case in which the walker is initialized on the walls of the "bucket", i.e., $x_0 > L$ (the case of $x_0 < -L$ is solved by symmetry), the Laplace domain propagator is

$$\tilde{\Pi} = \begin{cases} \dfrac{e^{-(x-x_0)/2l}}{\Gamma Q(\epsilon)}\left[e^{-Q(\epsilon)|x-x_0|/2l} + \dfrac{2\sqrt{\frac{4l\epsilon}{\Gamma}}\cosh 2\sqrt{\frac{\epsilon}{D}}L}{\kappa(\epsilon)}e^{-Q(\epsilon)(x+x_0-2L)/2l}\right] & x > L \\ 2\dfrac{e^{-(Q(\epsilon)-1)(x_0-L)/2l}}{\Gamma\kappa(\epsilon)}\left[(Q(\epsilon)-1)\sinh\sqrt{\frac{\epsilon}{D}}(x+L) + \sqrt{\frac{4l\epsilon}{\Gamma}}\cosh\sqrt{\frac{\epsilon}{D}}(x+L)\right] & x < |L| \\ 2\dfrac{e^{(x+x_0)/2l}}{\Gamma\kappa(\epsilon)}e^{Q(\epsilon)(x-x_0+2L)/2l}\sqrt{\frac{4l\epsilon}{\Gamma}} & x < -L \end{cases} \tag{17}$$

where we have suppressed the arguments of $\tilde{\Pi}$ and

$$Q(\epsilon) = \sqrt{1 + \frac{4l\epsilon}{\Gamma}}, \qquad \kappa(\epsilon) = 2\left(\frac{4l\epsilon}{\Gamma} - Q(\epsilon)\right)\sinh 2\sqrt{\frac{\epsilon}{D}}L + 2(Q(\epsilon) - 1)\sqrt{\frac{4l\epsilon}{\Gamma}}\cosh 2\sqrt{\frac{\epsilon}{D}}L$$

The form of eq 17 in the sloped regions of the potential corresponds well with their equivalent regions when under a V-potential. They are modified by functions of L and, in the limit $L \to \infty$, reduce to eq 5. The case where $L > x_0 > -L$, i.e., the walker is initialized on the bottom of the basket, is included in the Appendix.

The presence of the Laplace variable ϵ in two different forms, $1 + 4Dl\epsilon/\Gamma$ and ϵ/D, in eq 17 requires numerical methods to invert the transform. For this purpose we use standard inversion routines.[31,32] We exhibit the resulting time-domain propagator at four different dimensionless times in Figure 9.

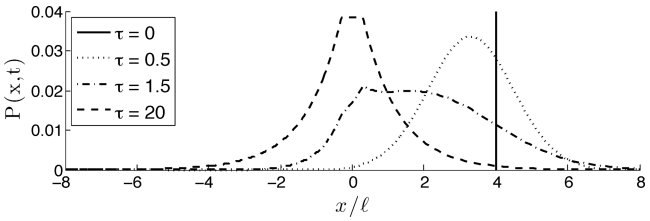

Figure 9. Counterpart of Figure 2 for the "bucket potential". The time-domain propagator is plotted at four values (0, 0.5, 1.5, 10) of the dimensionless time $\tau = t/\sqrt{2D/\Gamma^2}$ for an initial location of the walker at $x_0/l = 4$, and the bucket width as $L/l = 0.3$. The propagator behaves essentially as in Figure 2, but the steady state has a flat portion in the center. The transitioning of the intermediate Gaussian into the mod exponential with a flat central portion is already evident in the earlier time curve at $\tau = 1.5$.

Similar to the probability propagation of the V-potential, Figure 2, the propagator initially travels ballistically, undergoes a transition in shape, and then settles into the steady state distribution. The latter is a central plateau of width $2L = 6$ bracketed by decaying exponentials with characteristic width $l = 10$. The propagator of the "bucket" potential and that of the V-potential behave similarly in the outer regions of nonzero force, initially possessing a Gaussian shape before transitioning into a decaying exponential. The difference between the two lies in the central region, where the "bucket" propagator connects the probability values at the two points of discontinuity in an approximately linear fashion. This nearly linear form is due to the effects of diffusion under forced unequal boundary conditions. During the transition period, diffusion works to gradually equalize these two boundary probabilities, decreasing the steepness of the propagator.

The resulting relationship between $\langle x\rangle$ and $\langle v\rangle$ for the "bucket" potential is depicted in Figure 10. It is visually obvious

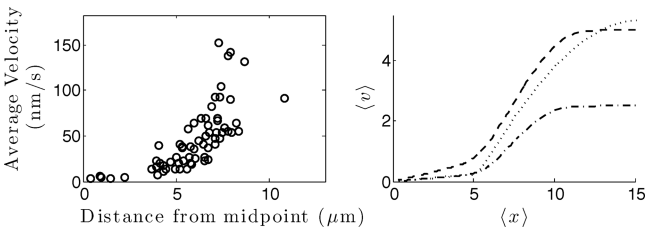

Figure 10. Qualitative comparison, as in Figure 6, of experimental observations from ref 30 (left panel is identical to that in Figure 6) to our theoretical predictions. The latter here are for the "bucket" potential for a few different values of its parameters (right panel). Considerable enhancement is seen in the qualitative agreement since the bucket potential is able to reproduce the central flat portion.

that there is much better agreement between experiment[30] and our calculations with the bucket potential than with the V-potential. The former retains the initial dormant behavior characteristic of the V-potential as well as the plunge, $\langle v\rangle \to 0$, when the walker interacts strongly with the discontinuities present in both potentials. As expected, the qualitative difference between the two lies in the location of this rapid decrease in speed. For the 'bucket' potential this plunge occurs

DOI: 10.1021/acs.jpcb.5b12548

in the periphery, as opposed to at the center, resulting in the addition of a central area of small or vanishing velocity. The presence of this low-velocity area results from the constant potential center, as the confinement increases the probability of locating the walker in the center where motion is dominated by diffusion.

6. CONCLUDING REMARKS

The primary goal of our analysis above was to obtain and examine propagator solutions of a time evolution equation, eq 2, which describes a random walk under confinement due to a V-potential, i.e., a potential which is (mod) linear in the distance of the walker from an attractive center. A secondary goal was to illustrate how the solutions may be applied to observations in principle. The analytic solutions we have obtained are (eq 5) in the Laplace domain and (eq 6) in the time domain. A numerical verification of eq 6 is shown in Figure 1. A graphical representation of the solution, provided in Figure 2, makes clear the shape-shifting of an initial $\delta-$ function distribution through ballistically moving Gaussians to the cuspy, mod exponential, steady state. We have also supplied explicit analytic expressions for the average position and average velocity of the walker (time derivative of the average position), eqs 9 and 10, respectively, and explored them graphically in Figures 3 and 4. The dependence of the average velocity on the average position is shown in Figure 5 for various values of the parameter α which is the ratio of the initial distance from the attractive center to the steady state width of the distribution.

Although the V-potential is linear in the distance of the random walker from the attractive center, its consequences for the motion are richer than those of the quadratic potential. The differences are detailed in section 3. Shape-shifting of the probability distribution is one such special characteristic of the V-potential equation. The dependence of the relation between velocity and position on the diffusion constant is another. The nonlinearity of the force with respect to the distance is responsible for this characteristic: the *force* is linear for the quadratic potential case.

We have indicated in sections 4 and 5 how our calculations could be applied to two unrelated systems. One of them concerns doped molecular aggregates, and the other concerns immunology. In the first, we calculated the quantum yield and examined an interesting nonmonotonicity effect which was the result of confinement. A realization of the system we have analyzed as an illustrative application requires that the experimentalist confine the excitation with the help of the V-potential. An electric field applied with opposite signs symmetrically about a location would make this possible if the moving particle is charged. Experimental observations[33] on the decrease of quantum yield on applying an electric field and related discussions by Hanson and others[34,35] may be of interest in this context. Alternatively, one may consider the moving particle to be not an excitation as in sensitized luminescence but an electron as in many related organic systems. In this case, τ will correspond not to a *radiative* lifetime but a lifetime against other types of capture processes in the system.

In the second application we have presented, we saw that our predictions for the time dependence of the velocity of the microclusters reproduced in a qualitative sense observations reported in the literature, but results for the velocity-position dependence were different qualitatively from the data. The difference was in the distance-independence of the velocity in the center region. Therefore, we showed how we can extend our calculations to the bucket potential case, i.e., a potential which is piecewise linear, with a flat shape in the center. This extension produced qualitatively compatible results. If we take the tentative point of view that invoking a V-potential Smoluchowski equation properly represents an approach based on a distance-independent force, we can conclude, as outlined in the paper, that our analysis shows that a pure distance-independent force cannot account fully for the observed TCR microcluster motion. Forces other than actin polymerization pushing against the cell membrane could be responsible for actin retrograde flow, or actin retrograde flow may not be the only driving force for microcluster centralization.[23,29]

APPENDIX

Bucket Potential Propagator for Walker Placed Initially in the Central Region

In our calculation of the propagator for the bucket potential we have given the analysis and the result in the text of the paper for initial placement of the walker in the walls of the bucket, i.e., for $|x| > L$, and mentioned that the case of initial placement on the floor of the bucket ($|x| < L$) is shown here. The latter expression follows.

$$\tilde{\Pi}(x, x_0, \epsilon) = \begin{cases} e^{-\left(1+\sqrt{1+\frac{4l\epsilon}{\Gamma}}\right)(x-L)/2l} \dfrac{\sqrt{1+\frac{4l\epsilon}{\Gamma}}+1}{4l\epsilon} \dfrac{\mathcal{P}(x_0, \epsilon)}{\mathcal{D}(\epsilon)} & x > L \\ \dfrac{\sqrt{1+\frac{4l\epsilon}{\Gamma}}+1}{\Gamma\sqrt{\frac{4l\epsilon}{\Gamma}}\,4l\epsilon} \dfrac{\mathcal{P}(x_0, \epsilon)\mathcal{M}(x, \epsilon)}{\mathcal{D}(\epsilon)} & L > x > x_0 \\ \dfrac{\sqrt{1+\frac{4l\epsilon}{\Gamma}}+1}{\Gamma\sqrt{\frac{4l\epsilon}{\Gamma}}\,4l\epsilon} \dfrac{\mathcal{P}(x, \epsilon)\mathcal{M}(x_0, \epsilon)}{\mathcal{D}(\epsilon)} & x_0 > x > -L \\ e^{\left(1+\sqrt{1+\frac{4l\epsilon}{\Gamma}}\right)(x+L)/2l} \dfrac{\sqrt{1+\frac{4l\epsilon}{\Gamma}}+1}{4l\epsilon} \dfrac{\mathcal{M}(x_0, \epsilon)}{\mathcal{D}(\epsilon)} & -L > x \end{cases} \tag{18}$$

Here

$$\mathcal{P}(x, \epsilon) = \left(\left(\sqrt{1+\frac{4l\epsilon}{\Gamma}}-1\right)\sinh\sqrt{\frac{\epsilon}{D}}(L+x) + \sqrt{\frac{4l\epsilon}{\Gamma}}\cosh\sqrt{\frac{\epsilon}{D}}(L+x)\right)$$

$$\mathcal{M}(x, \epsilon) = \left(\left(\sqrt{1+\frac{4l\epsilon}{\Gamma}}-1\right)\sinh\sqrt{\frac{\epsilon}{D}}(L-x) + \sqrt{\frac{4l\epsilon}{\Gamma}}\cosh\sqrt{\frac{\epsilon}{D}}(L-x)\right)$$

$$\mathcal{D}(\epsilon) = \sqrt{1+\frac{4l\epsilon}{\Gamma}}\sinh 2\sqrt{\frac{\epsilon}{D}}L + \sqrt{\frac{4l\epsilon}{\Gamma}}\cosh 2\sqrt{\frac{\epsilon}{D}}L \tag{19}$$

DOI: 10.1021/acs.jpcb.5b12548

AUTHOR INFORMATION

Corresponding Authors

*E-mail: mchase@unm.edu.
*E-mail: kspendie@uccs.edu.
*E-mail: kenkre@unm.edu.

Notes

The authors declare no competing financial interest.

ACKNOWLEDGMENTS

This work was supported in part by the Consortium of the Americas for Interdisciplinary Science and by the University of Colorado, Colorado Springs BioFrontiers Center. The authors thank Dr. Janis K. Burkhardt for discussions on T-cell receptor transport.

REFERENCES

(1) Wade, R. C.; Gabdoulline, R. R.; Lüdemann, S. K.; Lounnas, V. Electrostatic Steering and Ionic Tethering in Enzyme-Ligand Binding: Insights from Simulations. *Proc. Natl. Acad. Sci. U. S. A.* **1998**, *95*, 5942−5949.

(2) Livesay, D. R.; Jambeck, P.; Rojnuckarin, A.; Subramaniam, S. Conservation of Electrostatic Properties within Enzyme Families and Superfamilies. *Biochemistry* **2003**, *42*, 3464−3473.

(3) Ebeling, W.; Schweitzer, F.; Tilch, B. Active Brownian Walkers with Energy Depots Modeling Animal Mobility. *BioSystems* **1999**, *49*, 17−29.

(4) Aldana, M.; Dossetti, V.; Huepe, C.; Kenkre, V. M.; Larralde, H. Phase Transitions in Systems of Self-Propelled Agents and Related Network Models. *Phys. Rev. Lett.* **2007**, *98*, 095702 DOI: 10.1103/PhysRevLett.98.095702.

(5) Giuggioli, L.; Abramson, G.; Kenkre, V. M.; Parmenter, C.; Yates, T. Theory of Home Range Estimation from Displacement Measurements of Animal Populations. *J. Theor. Biol.* **2006**, *240*, 126−135.

(6) Reichl, L. E. *A Modern Course in Statistical Physics*; Wiley-VCH Verlag: Weinheim, 2009.

(7) Risken, H. *The Fokker-Planck Equation: Methods of Solution and Applications*; Springer-Verlag: Berlin, 1989.

(8) Smoluchowski, M. V. Drei Vortrage Uber Diffusion, Brownsche Bewegung und Koagulation von Kolloidteilchen. *Z. Phys.* **1916**, *17*, 557−585.

(9) Lamm, G.; Schulten, K. Extended Browian Dynamics Approach to Diffusion-Controlled Processes. *J. Chem. Phys.* **1981**, *75*, 365−371.

(10) Lamm, G.; Schulten, K. Extended Brownian Dynamics II. Reactive, Nonlinear Diffusion. *J. Chem. Phys.* **1983**, *78*, 2713−2734.

(11) Lamm, G. Extended Brownian Dynamics. III. Three-Dimensional Diffusion. *J. Chem. Phys.* **1984**, *80*, 2845−2855.

(12) Wolf, H. C. Energy Transfer in Organic Molecular Crystals: A Survey of Experiments. In *Advances in Atomic and Molecular Physics*; Bates, D. R., Eastermann, I., Eds.; Academic: New York, 1967; Vol. *3*, pp 119−142.

(13) Powell, R. C.; Soos, Z. G. Singlet Exciton Energy Transfer in Organic Solids. *J. Lumin.* **1975**, *11*, 1−45.

(14) Kenkre, V. M. The Master Equation Approach: Coherence, Energy Transfer, Annihilation, and Relaxation. In *Exciton Dynamics in Molecular Crystals and Aggregates*; Hoehler, G., Ed.; Springer Tracts in Modern Physics; Springer: Berlin, 1982; Vol. *94*.

(15) Roberts, G. E.; Kaufman, H. *Table of Laplace Transforms*; W. B. Saunders Company: Philadelphia, 1966.

(16) Spendier, K.; Sugaya, S.; Kenkre, V. M. Reaction-Diffusion Theory in the Presence of an Attractive Harmonic Potential. *Phys. Rev. E* **2013**, *88*, 062142.

(17) Kenkre, V. M.; Sugaya, S. Theory of the Transmission of Infection in the Spread of Epidemics: Interacting Random Walkers with and without Confinement. *Bull. Math. Biol.* **2014**, *76*, 3016−3027.

(18) Clayton, R. K. *Photosynthesis: Physical Mechanisms and Chemical Patterns*; Cambridge University Press: Cambridge, U.K., 1980.

(19) Monks, C. R.; Freiberg, B. A.; Kupfer, H.; Sciaky, H.; Kupfer, A. Three-Dimensional Segregation of Supramolecular Activation Clusters in T Cells. *Nature* **1998**, *395*, 82−86.

(20) Huppa, J. B.; Davis, M. M. T-Cell-Antigen Recognition and the Immunological Synapse. *Nat. Rev. Immunol.* **2003**, *3*, 973−983.

(21) Dustin, M. L.; Chakraborty, A. K.; Shaw, A. S. Understanding the Structure and Function of the Immunological Synapse. Cold Spring Harbor Perspect. *Biol.* 2010, *2*, DOI: 10.1101/cshperspect.a002311.

(22) Dustin, M. L.; Cooper, J. A. The Immunological Synapse and the Actin Cytoskeleton: Molecular Hardware for T Cell Signaling. *Nat. Immunol.* **2000**, *1*, 23−29.

(23) Babich, A.; Li, S.; O'Connor, R. S.; Milone, M. C.; Freedman, B. D.; Burkhardt, J. K. F-Actin Polymerization and Retrograde Flow Drive Sustained PLCγ1 Signaling during T Cell Activation. *J. Cell Biol.* **2012**, *197*, 775−787.

(24) Yu, C.; Fay, N. C.; Smoligovets, A. A.; Wu, H.; Groves, J. T. Myosin IIA Modulates T Cell Receptor Transport and CasL Phosphorylation during Early Immunological Synapse Formation. *PloS ONE* **2012**, *7*, 30704 DOI: 10.1371/journal.pone.0030704.

(25) DeMond, A. L.; Mossman, K. D.; Starr, T.; Dustin, M. L.; Groves, J. T. T Cell Receptor Microcluster Transport through Molecular Mazes Reveals Mechanism of Translocation. *Biophys. J.* **2008**, *94*, 3286−3292.

(26) Yu, Y.; Wu, H.; Kaizuka, Y.; Vale, R. D.; Groves, J. T. Altered Actin Centripetal Retrograde Flow in Physically Restricted Immunological Synapses. *PLoS One* **2010**, *5*, e11878.

(27) Pollard, T. D.; Berro, J. Mathematical Models and Simulations of Cellular Processes based on Actin Filaments. *J. Biol. Chem.* **2009**, *284*, 5433−5437.

(28) Cai, Y.; Biais, N.; Giannone, G.; Tanase, M.; Jiang, G.; Hofman, J. M.; Wiggins, C. H.; Silberzan, P.; Buguin, A.; Ladoux, B.; Sheetz, M. P. Nonmuscle Myosin IIA-Dependent Force Inhibits Cell Spreading and Drives F-Actin Flow. *Biophys. J.* **2006**, *91*, 3907−3920.

(29) Yu, Y.; Smoligovets, A. A.; Groves, J. T. Modulation of T Cell Signaling by the Actin Cytoskeleton. *J. Cell Sci.* **2013**, *126*, 1049−1058.

(30) Yokosuka, T.; Sakata-Sogawa, K.; Kobayashi, W.; Hiroshima, M.; Hashimoto-Tane, A.; Tokunaga, M.; Dustin, M. L.; Saito, T. Newly Generated T Cell Receptor Microclusters Initiate and Sustain T Cell Activation by Recruitment of Zap 70 and SLP-76. *Nat. Immunol.* **2005**, *6*, 1253−1262.

(31) Gaver, D. P., Jr Observing Stochastic Processes and Approximate Transform Inversion. *Oper. Res.* **1966**, *14*, 444−459.

(32) Abate, J.; Whitt, W. Unified Framework for Numerically Inverting Laplace Transforms. *INFORMS J. Comput.* **2006**, *18*, 408−421.

(33) Patel, J. S.; Hanson, D. M. Experimental Observations of the Effect of an Electric Field on Exciton Motion in Molecular Crystals. *J. Chem. Phys.* **1981**, *75*, 5203−5205.

(34) Hanson, D. M. Effect of an External Electric Field on Electronic Excitation Energy Transfer in Molecular Crystals. *Mol. Cryst. Liq. Cryst.* **1980**, *57*, 243−253.

(35) Harris, C. B.; Zwemer, D. A. Coherent Energy Transfer in Solids. *Annu. Rev. Phys. Chem.* **1978**, *29*, 473−495.

DOI: 10.1021/acs.jpcb.5b12548